Nanomaterial safety for microbially-colonized hosts: Microbiota-mediated physisorption interactions and particle-specific toxicity

Brinkmann, B.W.

Citation

Brinkmann, B. W. (2022, December 8). *Nanomaterial safety for microbially-colonized hosts: Microbiota-mediated physisorption interactions and particle-specific toxicity*. Retrieved from https://hdl.handle.net/1887/3494409

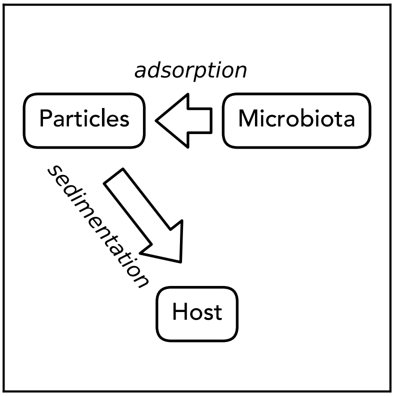
adsorption
Particles
Microbiota
sedimentation
Host

CHAPTER 3

Adsorption of titanium dioxide nanoparticles onto zebrafish eggs affects colonizing microbiota

Bregje W. Brinkmann
Wouter F. Beijk
Redmar C. Vlieg
S. John T. van Noort
Jorge Mejia
Julien L. Colaux
Stéphane Lucas
Gerda Lamers
Willie J. G. M. Peijnenburg
Martina G. Vijver

Published in *Aquatic Toxicology*, 232: 105744 (2021). DOI: 10.1016/j.aquatox.2021.105744
Data is available via *Mendeley Data*. DOI: 10.17632/2d4hcr5cb5.1

Abstract

Teleost fish embryos are protected by two acellular membranes against particulate pollutants that are present in the water column. These membranes provide an effective barrier preventing particle uptake. In this study, we tested the hypothesis that the adsorption of antimicrobial titanium dioxide nanoparticles onto zebrafish eggs nevertheless harms the developing embryo by disturbing early microbial colonization. Zebrafish eggs were exposed during their first day of development to 2, 5 and 10 mg $TiO_2 \cdot L^{-1}$ (NM-105). Additionally, eggs were exposed to gold nanorods to assess the effectiveness of the eggs' membranes in preventing particle uptake, localizing these particles by way of two-photon microscopy. This confirmed that particles accumulate onto zebrafish eggs, without any detectable amounts of particles crossing the protective membranes. By way of particle-induced X-ray emission analysis, we inferred that the titanium dioxide particles could cover 25–45 % of the zebrafish egg surface, where the concentrations of sorbed titanium correlated positively with concentrations of potassium and correlated negatively with concentrations of silicon. A combination of imaging and culture-based microbial identification techniques revealed that the adsorbed particles exerted antimicrobial effects, but resulted in an overall increase of microbial abundance, without any change in heterotrophic microbial activity, as inferred based on carbon substrate utilization. This effect persisted upon hatching, since larvae from particle-exposed eggs still comprised higher microbial abundance than larvae that hatched from control eggs. Notably, pathogenic aeromonads tolerated the antimicrobial properties of the nanoparticles. Overall, our results show that the adsorption of suspended antimicrobial nanoparticles on aquatic eggs can have cascading effects across different life stages of oviparous animals. Our study furthermore suggests that aggregation dynamics may occur that could facilitate the dispersal of pathogenic bacteria through aquatic ecosystems.

Keywords: Host-microbiota interactions; Cascading effects; Particle-Induced X-ray Emission; Two-photon multifocal microscopy; EcoPlate.

3.1 Introduction

Many vertebrate and invertebrate animals, including chordates, arthropods, echinoderms, cnidarians and mollusks, lay eggs that develop *ex vivo* in the water column. Their developing embryos are surrounded by envelopes of varying complexity, ranging from simple coats in cnidarians and nematodes, to acellular membranes with or without external jelly coating in chordates, arthropods, echinoderms and mollusks (Mazinni et al. 1984). In addition to the inner vitelline membrane, eggs of cephalopods, pterygotan insects and teleost fish are surrounded by an external chorion membrane. Together, the chorion and vitelline membranes protect the externally developing embryos against environmental stressors in the water column, including mechanical forces, predators, and pathogens (McMillan 2007).

Research on teleost fish eggs has shown that the chorion constitutes an effective physical barrier against the uptake of particulate pollutants. In medaka fish eggs, for instance, microplastic particles were found to adhere to the villi on the outside of the chorion, and could not be detected within eggs (Beiras et al. 2018). In zebrafish eggs, which do not comprise villi, microplastic particles from the water column attached to the chorion surface in a size-dependent manner. Relatively large microplastic particles, with a primary size of 10-20 μm, adhered in patches to the outside of the chorion, whereas smaller microplastic particles, with a primary size of 1-5 μm, covered the complete chorion surface (Batel et al. 2018). After hatching, only a few of these fluorescently labeled particles could be detected on the skin or in the intestinal tracts of larvae, suggesting that the uptake of the particles across the chorion surface was minor.

Similar to these micro-scaled particles, nanoparticles composed of polystyrene (Van Pomeren et al. 2017a; Lee et al. 2019; Duan et al. 2020), copper, zinc oxide, cobalt(II,III) oxide, nickel oxide (Lin et al. 2011; Brun et al. 2018), silicon dioxide (Fent et al. 2010), titanium dioxide, silver, gold and aluminum oxide (Osborne et al. 2013; Böhme et al. 2015), were found to accumulate on or in chorion structures of zebrafish eggs. A few studies have tracked particles moving through pores in the chorion membrane (Browning et al. 2009; Lee et al. 2013), or have identified nanoparticles in sections of zebrafish larvae that had been exposed to the particles prior to hatching (Lee et al. 2013, 2019). However, these first indications for potential uptake of particles across the chorion and vitelline membrane are hard to interpret due to limitations of the applied detection techniques, including the potential dissociation of the internalized fluorescent dyes that were used to localize particles (Schür et al. 2019), the potential impacts of sample fixation and sectioning on particle distribution, and the low z-confinement of the non-destructive imaging techniques that were used alternatively.

In addition to adverse effects of nanoparticles that may cross the protective membranes of zebrafish eggs, effects of particles that adsorb, and thereby accumulate, onto the chorion, could harm developing embryos. Such effects have for example been reported by Duan et al. (2020), who showed that micro- and nanoplastic particles can block the pores of zebrafish eggs, possibly lowering the oxygen supply to the embryo, resulting in hypoxia. The attached particles moreover caused delayed hatching of the embryos. Furthermore, indirect effects of particle adsorption have been described by Batel et al. (2018), who demonstrated that toxic compounds can leach out of chorion-attached polystyrene particles, onto the developing embryos. A parallel concern, posed by Böhme (2015), is the release of toxic metal ions into zebrafish eggs from chorion-attached metal nanoparticles. A fourth and hypothetical effect of chorion-attached nanoparticles, is the potential of these particles to interfere with establishing host-microbiota interactions, in particular in case the adsorbed particles exhibit antimicrobial activity. The chorion constitutes the first site of microbial colonization in developing zebrafish. After hatching, the chorion microbial community is assumed to play a key role in colonization of the initially sterile, pre-hatch embryo (Llewellyn et al. 2014). Hence, impacts of antimicrobial nanoparticles on chorion-attached microbial consortia may have cascading effects on the composition and functioning of larval microbiota. This is of concern, since already at the larval stage, microbiota is essential to zebrafish health, promoting epithelial proliferation, beta cell expansion and normal neurobehavioral development (Rawls et al. 2004; Hill et al. 2016; Phelps et al. 2017).

In this study, we investigate the hypothesized effects of nanoparticles on establishing zebrafish-microbiota interactions, focusing on the impacts of titanium dioxide nanoparticles ($nTiO_2$). These particles are amongst the most commonly applied antimicrobial metal nanoparticles on the market (Eduok and Coulon 2017), and have already been found to adsorb rapidly onto zebrafish eggs (Shih et al. 2016). We take a three-step approach to study potential adverse effects of $nTiO_2$ on zebrafish colonizing microbiota. Firstly, we investigate how $nTiO_2$ accumulates on zebrafish eggs, quantifying the total amount of titanium sorbed on zebrafish eggs using Particle-Induced X-ray Emission (PIXE) analysis (Lozano et al. 2012). We furthermore assess the effectiveness of the chorion barrier against particle uptake by localizing gold nanorods (nAu) on zebrafish eggs by way of two-photon microscopy. This detection method is non-destructive, highly sensitive and independent of potentially dissociating particle dyes. Secondly, we explore how $nTiO_2$ affects the survival of microbiota on the zebrafish chorion, combining culture-independent imaging techniques and culture-based microbiology techniques. Thirdly, we infer if impacts on egg microbiota can have cascading effects to microbiota of the larval life stage when particle exposure is discontinued, based on approximation of total microbiota abundance and carbon substrate utilization profiles of eggs and larvae. Altogether, these experiments shed light on potential consequences of nanoparticle adsorption on establishing host-microbiota interactions in aquatic oviparous animals.

3.2 Materials and methods

3.2.1 Nanoparticle dispersions

Titanium dioxide nanoparticles ($nTiO_2$) of series NM-105, with primary particles sizes around 15–24 nm, in rutile (12–19 %) and anatase (81–88 %) crystalline phase (Rasmussen et al. 2014), were purchased from the European Commission's Joint Research Centre (Ispra, Italy). For particle localization experiments (section 3.2.5), cetyltrimethylammonium bromide (CTAB)- and polyvinylpyrrolidone (PVP)-capped gold nanorods (nAu) with a diameter of 10 nm, a length of 45 nm and peak surface plasmon resonance at 850 nm, were purchased from Nanopartz (Loveland, USA). For analyses of microbiota composition (section 3.2.8), silver nanoparticles with a primary particle size of 15 nm (series NM-300K; Klein et al. 2011), kindly provided by RAS AG (Regensburg, Germany), were used as a positive control.

Nanoparticle dispersions were prepared in egg water (60 $mg \cdot L^{-1}$ Instant Ocean artificial sea salts in demi water; Sera GmbH, Heinsberg, Germany). Stock dispersions with a concentration of 100 $mg\ TiO_2 \cdot L^{-1}$, 5 $mg\ Au \cdot L^{-1}$ (CETAB-capped nAu), 0.5 $mg\ Au \cdot L^{-1}$ (PVP-capped nAu), and 100 $mg\ Ag \cdot L^{-1}$, were stabilized for 10 min in an ultrasonic bath (USC200T; VWR, Amsterdam, The Netherlands) at an acoustic power of 12 W, determined following the sonicator calibration standard operation procedure (SOP) delivered in EU FP7 project NANoREG (v 1.1; Jensen et al. 2018). Immediately thereafter, stock dispersions were diluted to obtain exposure concentrations 0, 2, 5 and 10 $mg\ TiO_2 \cdot L^{-1}$; 0, 0.03 and 0.1 $mg\ Au \cdot L^{-1}$; and 0 and 0.25 $mg\ Ag \cdot L^{-1}$.

Primary particle size and shape of $nTiO_2$ were characterized by way of transmission electron microscopy (TEM). We applied 5 µL of a 10 $mg\ TiO_2 \cdot L^{-1}$ $nTiO_2$ dispersion onto a 200 mesh carbon-coated copper TEM grid, and the grid was incubated for > 24 h to dry. Thereafter, images from the grid were acquired at 150,000 times magnification using a 100 kV JEOL (Tokyo, Japan) 1010 transmission electron microscope. The width and length of 30 particles were measured using ImageJ (v. 2.0.0; Abràmoff et al. 2004).

The stability of the $nTiO_2$ dispersions was assessed based on zeta potential (ZP) and hydrodynamic size measurements (z-average size) after 0, 2 and 24 h of incubation in egg water, using a Zetasizer Ultra instrument (Malvern Panalytical, Malvern, UK). We applied the Smoluchowski formula to derive ZP approximations from electrophoretic mobility measurements. The refractive index and absorption value were set to 2.49 and 0.01 respectively, according to Rasmussen et al. (2014). We performed 10 runs for each of the 3 repeated measurements of hydrodynamic size per sample (*n*=3). All other procedures were adopted from the standard operating procedure developed for dynamic light scattering (DLS) analyses in NANoREG (Jensen 2018a).

The sedimentation rate of $nTiO_2$ aggregates was determined in 15 mL, 16.9 mm-diameter conical tubes comprising 9 mL of 2, 5 and 10 mg $TiO_2 \cdot L^{-1}$ (*n*=3). Following 0, 2, and 24 h of incubation, the center 3 mL of the column was sampled. The samples were acidified by adding 0.3 mL of 96 % H_2SO_4, 0.3 mL of 85 % H_3PO_4 and 0.3 mL of 65 % HNO_3, and digested by ultrasonication for 1h at 50 °C in an ultrasonic bath. Titanium concentrations in acid-digested samples were measured by inductively coupled plasma optical emission spectrometry (ICP-OES), using a 5100 ICP-OES spectrometer (Agilent Technologies, Santa Clara, USA).

For characterization of primary particle characteristics and stability of the applied batch of nAu and nAg, we refer to Van Pomeren et al. (2019) and Brinkmann et al. (2020), respectively.

3.2.2 Nanoparticle exposures

Zebrafish eggs were obtained by crossing AB×TL wildtype zebrafish, following standard procedures described in 'The zebrafish book' (https://zfin.org). Adult zebrafish were housed at Leiden University's zebrafish facility at 28 °C in a 14 h:10 h light:dark-cycle. Animal welfare was surveyed by the Animal Welfare Body of Leiden University, and complied with Dutch national regulation on animal experimentation ('Wet op de dierproeven' and 'Dierproevenbesluit 2014'), and European animal welfare regulations (EU Animal Protection Directive 2010/63/EU).

Zebrafish eggs were exposed to nanoparticle dispersions in the 24-well plate setup introduced for nanotoxicity testing by Van Pomeren et al. (2017b). Ten eggs were exposed to 2 mL of exposure medium per 17.5 mm-diameter well from 0 to 1 day post-fertilization (dpf) at 28 °C. Considering the UV-induced toxicity of $nTiO_2$ (Jovanović 2015), well plates were placed under a blacklight (F15W/T5/BL359; Sylvania, Amsterdam, The Netherlands) at a 12 h:12 h light:dark-regime. The blacklight had a UV-A irradiance optimum around 380 nm of 3–6 $\mu W \cdot cm^{-2} \cdot nm^{-1}$ (Fig. S1). Exposures to nAu were performed without UV-irradiation, in the dark.

Eggs that had been exposed from 0 to 1 dpf to $nTiO_2$, nAg or no nanoparticles, were used to investigate potential cascading effects (section 3.2.7 and section 3.2.8). To this end, the eggs were rinsed thrice with egg water immediately following the 0 to 1 dpf exposure. Subsequently, the eggs were transferred to 24-well plates, comprising 10 eggs and 2 mL egg water per well. Incubation took place in the dark at 28 °C until hatching. Possibly as a side-effect of the initial UV-radiation from 0 to 1 dpf, part of the embryos of all treatment groups died or did not hatch from 1 to 3 dpf (Table S1). As a consequence, three instead of four biological replicates were included in analyses of microbiota carbon substrate utilization (section 3.2.8). Chorions of embryos that did not hatch naturally before the end of day 3 were removed manually. Thereafter, egg water was refreshed, and incubation was continued until analyses of larval microbiota at 5 dpf.

In order to verify whether the exposure concentrations of nTiO$_2$ were sublethal to zebrafish larvae, 3 dpf-larvae were exposed for 48 h to 0, 10, 30, 35, 50 and 100 mg $TiO_2 \cdot L^{-1}$ in the 24-well setup described above. Following 24 h of exposure, dead larvae were removed from the wells and exposure media were refreshed. Mortality was scored at 24 h and 48 h of exposure. Following the same procedure, the exposure concentration of nAg (0.25 mg $Ag \cdot L^{-1}$), used as positive control, has already been found to be sublethal to zebrafish larvae (Brinkmann et al. 2020).

3.2.3 Quantification of sorbed titanium

The total amount of sorbed titanium (Ti) of zebrafish eggs was quantified by way of PIXE analysis. This approach allowed to detect 17 additional elements, which were phosphorus, chloride, potassium, sulfur, sodium, magnesium, manganese, calcium, silicon, iron, cobalt, chromium, zinc, aluminum, nickel, copper and vanadium. To prepare the sample material for analysis, 5–40 zebrafish eggs of each exposure concentration were gently rinsed thrice with 5-10 mL egg water immediately following exposure in order to remove loosely attached particles (n=6). Subsequently, the eggs were frozen in 1 mL egg water at -20 °C (5 of 6 replicates) or they were frozen without egg water at -20 °C (1 of 6 replicates), and were lyophilized overnight.

The lyophilized zebrafish eggs were applied onto a cylindrical sample holder consisting of three layers: a vitreous carbon substrate at the bottom, followed by a ~40 nm-thick layer of gold (theoretical thickness = 77 ± 8 $\mu g \cdot cm^{-2}$; mean ± standard error of the mean (SEM)), and a final piece of carbon tape on top. The sample material was deposited inside of a 3 mm-diameter hole in the center of the carbon tape. The gold layer, which was applied onto the carbon substrate using a physical vapor deposition system, allowed to determine the thickness of the applied sample material.

For analysis, the sample holder was placed into a vacuum chamber. An incident 2.5 MeV proton beam with a diameter of ~1 mm was directed at the analysis chamber in a 30° angle. A magnetic filter was applied to remove the flux of backscattered protons. X-rays were collected by an Ultra-LEGe detector mounted at a 135 ° angle to the incident beam direction with a magnetic filter to remove the flux of backscattered protons. Backscattered particles were collected by two passivated implanted planar silicon detectors mounted at 165° and 135° to the incident proton beam. Measurements on 4 Certified Reference Materials (MicaMg, MAN, BEN, and DRN), performed at 2.5 MeV, indicated that the energy resolution of the system was excellent, averaging 126.6 ± 1.5 eV (mean ± SEM) measured on the Fe Kα line.

Elastic backscattering spectrometry spectra were reduced with DataFurnace software (calculation code: ndf v.9.6i, graphical interface: windf 9.3.94) (Barradas and Jeynes 2008), and PIXE spectra were analyzed using GUPIX software (by J.L. Campbell; v. 2.2.0; http://pixe.physics.uoguelph.ca/gupix/main/). Masses were corrected for the elemental masses in 1 mL egg water, according to the elemental compositions of Instant Ocean salts determined by Atkinson and Bingman (1996). Elemental masses were expressed as ng per zebrafish egg, assuming that the dry mass of a zebrafish egg at 1 dpf approximates 70 µg (Hachicho et al. 2015).

3.2.4 Calculation of aggregate coverage on eggs

In order to estimate the total surface area of zebrafish eggs that could be covered by $nTiO_2$ aggregates at the measured concentrations of sorbed $nTiO_2$, we first calculated the maximum number of aggregates (N) that could theoretically attach to zebrafish eggs in one monolayer of aggregates in a hexagonal close-packing (packing factor = $\frac{\pi}{2\sqrt{3}}$), assuming that both the zebrafish eggs and aggregates are spherically shaped:

$$N = \frac{4\pi r_{egg}{}^2}{\pi r_{aggregate}{}^2} \times \frac{\pi}{2\sqrt{3}} \qquad \text{(eq 3.1)}$$

The radius of the aggregates ($r_{aggregate}$) was derived from DLS measurements (section 3.2.1) using the hydrodynamic (*z-average*) size estimates obtained at the start of exposure, and the radius of zebrafish eggs (r_{egg}) was derived from confocal microscopy images (section 3.2.6). Subsequently, the mass of this $nTiO_2$-aggregate monolayer (m_N) was calculated following:

$$m_N = \frac{4}{3}\pi r_{aggregate}{}^3 \times N \times \rho_{aggregate} \qquad \text{(eq 3.2)}$$

where the effective density of aggregates ($\rho_{aggregate}$) was calculated based on the average area fraction of aggregates covered by particles ($\overline{A_{particle}}$) in TEM pictures (Fig. S2) and the particle density ($\rho_{particle}$) of 4.26 $g{\cdot}cm^{-3}$ determined by Teleki et al. (2008), following:

$$\rho_{aggregate} = \overline{A_{particle}}^{\,3} \times \rho_{particle} \qquad \text{(eq 3.3)}$$

Finally, the fraction of the surface area of zebrafish eggs that was covered by $nTiO_2$

aggregates was inferred by dividing the mass of one monolayer of $nTiO_2$ aggregates by the measured mass of $nTiO_2$ per egg. For comparison with previous research, the same calculation was performed for primary particles, using the primary particle radius determined by TEM (section 3.2.1) and primary particle density determined by Teleki et al. (2008), instead of aggregate radius and effective aggregate density.

3.2.5 Localization of nanoparticles on eggs

We localized nAu on zebrafish eggs by way of two-photon microscopy to assess the effectiveness of the chorion barrier against nanoparticle uptake. These rods can be detected with high sensitivity at an excitation wavelength of 850 nm, owing to their plasmon-enhanced two-photon luminescence (TPL) at this wavelength. Zebrafish eggs were mounted onto a glass slide with 1.5 % low melting agarose (CAS 39346-81-1; Sigma-Aldrich, Darmstadt, Germany) comprising 200 $\mu g \cdot mL^{-1}$ of the anesthetic tricaine (3-amino-benzoic acid; Sigma-Aldrich) in egg water. As soon as the agarose had solidified, samples were excited with a femtosecond pulsed Ti:Sa laser (Chameleon Ultra; Coherent, Santa Clara, CA, USA), operating in spiral scanning mode (n=14, A=8.912 µm, σ_G=21.166 µm; Van den Broek et al. 2013) at 4 Hz per frame, with an exposure time of 0.2 s. The microscope was equipped with a 25×/1.10 NA objective (CFI75 Apochromat 25XC W; Nikon, Tokio, Japan).

Excitation spectra were acquired between 670 nm and 900 nm at 1 nm-resolution. Laser power was set to 1.44 mW per focus. In order to obtain z-projections, optical sections of control, 0.03 mg $Au \cdot L^{-1}$ exposed and 0.1 mg $Au \cdot L^{-1}$ exposed samples were obtained at an excitation wavelength of 830 nm and with a 0.3 µm pitch over a total sample thickness of 234 µm. The exposure time was set to 0.2 s for control and 0.1 mg $Au \cdot L^{-1}$ exposed samples, and to 0.1 s for 0.03 mg $Au \cdot L^{-1}$ exposed samples. Transmitted light images were obtained using a light emitting diode. Maximum intensity projections of optical sections were computed using ImageJ.

3.2.6 Microscopy-based analysis of zebrafish egg microbiota

The survival of microbiota on eggs was studied using culture-independent imaging techniques, in combination with culture-based microbiota isolation and identification (section 3.2.7). For imaging analysis, we used the BacLight fluorophore mixture (Molecular Probes, Eugene, Oregon), comprising the green fluorescent dye Syto-9 (0.12 µM), labelling all microbes, and the red fluorescent dye propidium iodide (0.73 µM), labelling microbes with damaged cell membranes. Eggs were stained for 15 min at room temperature in 15 mL conical tubes comprising 1–1.5 mL of the fluorophore mixture in egg water (3–6 eggs per tube). Afterwards, eggs were rinsed thrice with 5–10 mL egg water. Fluorescently labeled and rinsed eggs were mounted on a glass bottom petri dish (WilCo-dish; Willco Wells, Amsterdam, The Netherlands), by covering the eggs with 1.5 % low melting agarose (Sigma-Aldrich) containing 400 μg·mL^{-1} tricaine (Sigma-Aldrich) in egg water. In total, 45 eggs were imaged of the 0 and 10 mg TiO_2·L^{-1} exposures, and 24 eggs were imaged of the 2 and 5 mg TiO_2·L^{-1} exposures.

Labelled microbes were detected using an inverted LSM 880 confocal laser scanning microscope (Zeiss, Oberkochem, Germany) equipped with EC Plan-Neofluar 20×/0.50 NA M27 objective (Zeiss). Syto-9 was excited at 488 nm and detected using a 505–530 BP filter. Propidium idodide was excited sequentially at 543 nm and was detected in a separate channel using a 560 LP filter. From each egg, fifteen consecutive, 2.27 μm-thick optical slices were acquired, starting at the center bottom of the eggs. Each of the optical slices had a surface of 322.56 μm × 322.56 μm. Line averaging was set to 4 to reduce noise.

Image stacks were imported into MATLAB (v. R2020a) using the TIFF-Stack module developed by Muir and Kampa (2015), and were processed in five steps using the DipImage plugin (v. 2.9; www.diplib.org/dipimage). Firstly, we applied a mask to the scanned volume, in order to exclude autofluorescence from yolk globules. The mask corresponded to the volume of a sphere with the same radius as zebrafish eggs (0.6 mm), which was shifted two 2.27 μm-thick optical sections downwards relative to the eggs. Secondly, optical sections were combined by way of maximum intensity projection. Thirdly, projections were converted to binary images, applying a threshold equal to the mean signal of the concerning projection, plus thrice the standard deviation of this signal. Fourthly, at all locations where both Syto9 (all microbes) and propidium iodide (dead microbes) were detected, the signal in the Syto9 projection was set to 0. As a result, signal in Syto9 projections corresponded to live microbes. Finally, binary images were exported in TIFF format to ImageJ, where impulse noise was removed from images using a median filter with a radius of 1 pixel. The total area fraction covered by live microbes (Syto9 projections) or dead microbes (propidium iodide projections) was quantified using ImageJ. Regions with signal that clearly did not correspond to the size and shape of microbes, were omitted. The median surface (and interquantile range (IQR)) of the omitted regions was 0.21 % (IQR= 0–0.71 %) in controls, 0.36 % (IQR= 0–0.57 %) at 2 mg TiO_2·L^{-1}, 0.40 % (IQR=0–1.1 %) at 5 mg TiO_2·L^{-1} and 0.21% (IQR=0–0.60 %) at 10 mg TiO_2·L^{-1}.

3.2.7 Culture-based analysis of egg and larval microbiota

In addition to culture-independent imaging analysis (section 3.2.6), we determined the number and identity of bacterial isolates on nutrient-rich Lysogeny broth (LB) medium as an approximation of microbiota abundance and composition. Microbiota was isolated from zebrafish eggs and larvae using a tissue homogenizer (Bullet Blender model Blue-CE; Next Advance, New York, USA). From each exposure, 3 embryos or 3 larvae were transferred to a 1.5 mL SafeLock microcentrifuge tube (Eppendorf, Nijmegen, The Netherlands) comprising 200 μL autoclaved egg water and 6 zirconium oxide beads (1.0 mm-diameter; Next Advance). After initial cooling on ice for 2 min, performed to anaesthetize embryos and larvae, samples were homogenized for 15 s at speed 7. The homogenate was cooled on ice for 10 s immediately thereafter, to minimize potential damage to microbes due to heat generated in the tissue homogenizer. Subsequently, the homogenization and cooling steps were repeated seven times, to obtain a total homogenization time of 2 min. The sample homogenate was diluted 10, 100 and 1000 times in autoclaved egg water. Of each dilution, and of the non-diluted homogenate, 50 μL was plated on solid LB growth medium. After two days of incubation at 28 °C, colony-forming units (CFUs) were counted as a measure of live microbiota abundance. Incubations were continued for 2 more days, and any additional colonies were counted. Dilutions comprising 22–240 CFUs were used to assess microbiota abundance.

In order to identify what bacterial species occurred on zebrafish eggs, 10 CFUs isolated from $nTiO_2$-exposed and non-exposed zebrafish eggs (1 dpf) were selected for 16S rRNA-based identification (n=3). We aimed to identify as many different species as possible, and hence selected equal numbers of CFUs of each of the colony morphologies that appeared on LB plates. Colonies were selected from 1:10 dilutions of control samples, and 1:100 dilutions of exposed samples, comprising similar CFU counts (76 ± 21 CFUs per plate; mean ± SEM), to exclude potential dilution effects on microbial composition. Of each selected colony, a 1505-nt fragment of the 16S rRNA gene was amplified using universal bacterial primers (27F and 1492R). Polymerase-chain reactions, Sanger sequencing and species identification were performed as we described before (Brinkmann et al. 2020).

For two reasons, the above methods used to isolate, quantify and identify zebrafish microbes, likely underestimate microbiota abundance and diversity. Firstly, the isolation method is detrimental to a small fraction of the microbiota, as determined in our previous study (Brinkmann et al. 2020). Secondly, some bacteria may require different nutrients than present in LB medium, longer incubation times than 4 days, or alternative incubation conditions. For this reason, both the number and identity of microbial isolates as determined in this study, should be interpreted as a relative rather than an absolute representation of zebrafish larvae associated microbiota across the different experimental treatments.

3.2.8 Carbon-substrate utilization profiles of eggs and larval microbiota

We used EcoPlates (Biolog, Hayward, California) to characterize the carbon substrate utilization of zebrafish microbiota. These plates are commercially available and comprise 96-wells with 31 different lyophilized carbon substrates and 1 blank in triplo. In addition to the carbon substrates, each EcoPlate well comprises the redox dye tetrazolium violet that can be used to quantify the utilization of the corresponding carbon substrates colorimetrically at a wavelength of 590 nm.

Microbiota for EcoPlate analyses was isolated from 12 larvae of each biological replicate (*n*=3, three tubes with four larvae each), following the procedure described in section 3.2.7. Larvae homogenate was pooled and diluted with 14.4 mL sterile egg water. We inoculated EcoPlates with 100 µL of diluted microbiota per well, and incubated the plates in the dark at 28 °C. In order to test if zebrafish enzymes contribute to color development on EcoPlates, homogenate of germ-free zebrafish larvae at 5 dpf, obtained following Brinkmann et al. (2020), was inoculated on an additional EcoPlate. The optical density (*OD*) of EcoPlates was measured daily, from 1 to 4 days of incubation, at 590 nm with an Infinite M1000 plate reader (Tecan, Männedorf, Switzerland).

Ecoplate substrate utilization profiles of zebrafish larvae microbiota were compared between the different experimental conditions, based on the rate of color development between 1 and 2 days of incubation, expressed in *OD* units per hour. During this part of the incubation, color development increased linearly (Fig. S3). Additionally, four functional community parameters were derived from EcoPlate well-color development. Firstly, the average well color development (*AWCD*) was calculated following (Garland and Mills 1991):

$$AWCD = \frac{\sum_{i=1}^{S} OD_i - OD_c}{31} \qquad \text{(eq 3.4)}$$

where OD_i is the well color development for the *i*th carbon substrates *S*, and OD_c is the color development in the control well without carbon substrate. In some cases, where $OD_i<OD_c$, this produced negative values, which were set to 0. Secondly, Ecoplate carbon substrate utilization richness (*R*) was calculated as the sum of all substrates where $OD_i > 0.25$, according to Sillen et al. (2015):

$$R = \sum_{\{i \mid (OD_i > 0.25)\}}^{S} S(i) \qquad \text{(eq 3.5)}$$

Thirdly, color development was normalized, and the Shannon diversity index (*H'*) was calculated as a measure of the diversity in utilized carbon substrates, following:

$$p_i = \frac{\sum_{i=1}^{S} OD_i - OD_c}{AWCD} \qquad \text{(eq 3.6a)}$$

$$H' = -\sum_{i=1}^{S}(p_i \ \ln p_i) \qquad \text{(eq 3.6b)}$$

where p_i represents the normalized color development. Fourthly, to characterize the evenness of carbon utilization across the different substrates, the Pielou's evenness index (*J'*) was calculated as:

$$J' = \frac{H'}{\ln (R)} \qquad \text{(eq 3.7)}$$

3.2.9 Statistical analyses

Statistical analyses were performed in R (v. 3.6.3; www.r-project.org). Mean and SEM are presented, calculated using the 'bear' package (v. 2.8.7; pkpd.kmu.edu.tw/bear). In case data did not follow a normal distribution, median and IQR values are presented. Figures were plotted using Python (v. 3.6.5) with packages 'numpy' (v.1.19.1), 'pandas' (v.0.23.3), 'matplotlib' (v.3.1.3), and 'scipy' (v.1.5.0).

An overview of the applied statistical models is presented in Table 3.1. Only significant interactions between explanatory variables were included in statistical models. In case explanatory variables were factorial, two-way ANOVA tests were combined with Tukey's HSD post-hoc test. Spearman rank correlations between elemental concentrations of the 18 elements determined by PIXE analysis, were computed using the 'Hmisc' package (v. 4.4–0). For CLSM and EcoPlate data, data included repeated measurements from the same exposure well (CLSM data) or EcoPlate. We accounted for this in a nested ANOVA design using the 'nlme' (v.3.1–144) package, including exposure well or EcoPlate as the random variable. Cluster analyses of EcoPlate data were performed using the 'vegan' package (v.2.5–6), based on Bray-Curtis dissimilarity matrices, computed using the *vegdist* function. We compared dissimilarity matrices by way of Permutational multivariate analysis of variance (PERMANOVA) with 999 permutations, using the *adonis* function. Permutations were restricted to the exposure treatment groups and were not allowed to occur among replicates of the same exposure. Clusters were visualized in non-metric multidimensional scaling (nMDS) plots, obtained using the *metaMDS* function.

For all models, model assumptions were checked by inspecting the model's diagnostic Q-Q plot and residuals vs. fit plot. Equality of variance between groups was tested using Levene's test from the 'car' package (v. 3.0–7). For cluster analyses, the *betadisper* function was used to test if multivariate spread across matrices was similar. The Shapiro-Wilk test for normality was performed to test if residuals followed a normal distribution. In several cases, square-root, logarithmic or rank transformation was required to ensure this (Table 3.1). Skewness was quantified using the 'e1071' package (v. 1.7–3).

Table 3.1: Performed statistical analyses. *Abbreviations*: ANOVA, analysis of variance; AWCD, average well-color development; CLSM, confocal laser scanning microscopy; CFU, colony-forming unit; DLS, dynamic light scattering; log, logarithmic; PERMANOVA, permutational analysis of variance; PIXE, particle-induced X-ray emission; sqrt, square root; ZP, zeta potential.

Experimental analysis	*Response variable*	*Statistical model*	*Explanatory variables*	*Significant interaction*	*Transformation*
DLS	Hydrodynamic size	Two-way ANOVA	Incubation time × exposure concentration	yes	none
	ZP	Two-way ANOVA	Incubation time + exposure concentration	no	none [a]
PIXE	TiO_2 concentration per egg	Two-way ANOVA	Exposure concentration [b]	N.A.	log
	Elemental concentrations per egg	Spearman rank correlations	N.A.	N.A.	none
CLSM	Total microbial cover	Nested ANOVA	Exposure concentration	N.A.	sqrt
	Dead or live microbial cover	Nested ANOVA	Fraction (dead or live)	N.A.	log (at 0 mg $TiO_2 \cdot L^{-1}$), none (at 2 mg $TiO_2 \cdot L^{-1}$), sqrt (at 5 and 10 mg $TiO_2 \cdot L^{-1}$)[c]
CFU abundances	CFU count	Two-way ANOVA	Life stage + exposure concentration	no	log
EcoPlate	Carbon substrate profile	PERMANOVA	Life stage × exposure concentration	yes	none
	AWCD	Nested ANOVA	Life stage + exposure concentration	no	none
	Richness	Nested ANOVA	Life stage + exposure concentration	no	none
	Shannon diversity index	Nested ANOVA	Life stage + exposure concentration	no	none
	Evenness	Nested ANOVA	Life stage + exposure concentration	no	log (data without nAg) none (data with nAg)

[a] Only if one outlier with positive ZP was excluded, residuals followed a normal distribution. As this did not affect the results of the ANOVA test, the outlier was not excluded from the model.

[b] Exposure concentration was included as a factor, in order to obtain a normal distribution of model residuals. Despite log transformation of the data, the distribution of variance over the different exposure concentrations remained slightly unequal ($F_{3,20}$=3.61, *p*=0.03), and hence results should be treated with care.

[c] Residuals from the 10 mg $TiO_2 \cdot L^{-1}$ model deviated slightly from a normal distribution according to a Shapiro-Wilk test for normality (W=0.98, *p*=0.03). As both histogram shape and skewness (-0.02) did not indicate clear deviations from normality, the ANOVA results are presented nonetheless.

3.3 Results

3.3.1 Nanoparticle shape, size and stability

Primary $nTiO_2$ particles had irregular, angulated shapes with a width of 21.3 ± 1.2 nm and a length of 28.0 ± 1.5 nm (n = 30) (Fig. 3.1a). Following dispersion, the particles formed aggregates with a hydrodynamic size of 1.31 ± 0.17 µm, irrespective of the exposure concentration (Table 3.2). Over the 24-h exposure time, the size of the aggregates changed ($F_{1,23}$=14.6, p=0.0009) in a concentration-dependent manner ($F_{1,23}$=11.3, p=0.003), reaching hydrodynamic sizes of 1.22 ± 0.38 µm, 2.50 ± 0.89 µm, and 4.08 ± 1.08 µm at the end of exposure, at the nominal exposure concentrations of 2, 5 and 10 mg $TiO_2 \cdot L^{-1}$, respectively ($F_{1,23}$=6.3, p=0.02). The sedimentation analysis indicated that all aggregates had reached the bottom of the well in 14.0 h, 11.4 h and 10.5 h at the 2, 5 and 10 mg $TiO_2 \cdot L^{-1}$ exposures, respectively (Fig. S4). This suggests that particle stability decreased at increasing exposure concentrations. Accordingly, the zeta potential of aggregates was concentration-dependent ($F_{1,23}$=33.3, p=$6.1 \cdot 10^{-6}$), averaging -19.1 ± 0.30 mV, -14.2 ± 0.92 mV, and -10.0 ± 1.7 mV at nominal exposure concentrations of 2, 5 and 10 mg $TiO_2 \cdot L^{-1}$, respectively. At all concentrations, the zeta potential of the aggregates did not change over time ($F_{1,23}$=1.5, p>0.05) (Table 3.2).

3.3.2 Sorption of nanoparticles to zebrafish eggs

Akin to the aggregation of $nTiO_2$, sorption of $nTiO_2$ to zebrafish eggs was concentration-dependent ($F_{3,20}$ = $1.0 \cdot 10^3$, p< $2.0 \cdot 10^{-16}$; Fig. 3.1b). No titanium could be detected in zebrafish eggs that were not exposed to $nTiO_2$ (with a limit of detection of 3.6 ± 1.0 ng per egg). A lower concentration of titanium was detected at the exposure concentration of 2 mg $TiO_2 \cdot L^{-1}$, averaging 30.4 ± 9.0 ng per egg, than at the highest two

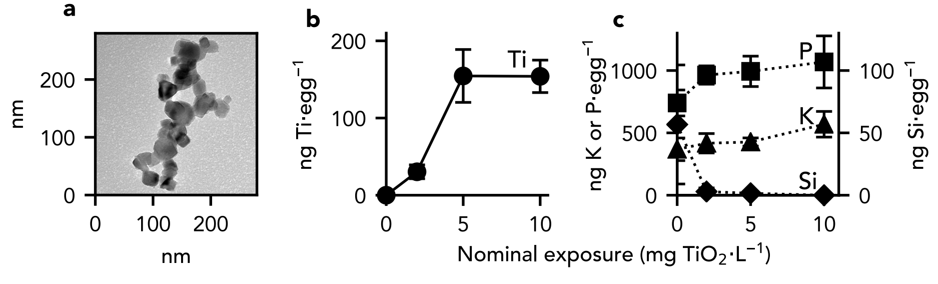

Figure 3.1: *Quantification of the sorption of titanium (Ti) and correlated elements on zebrafish eggs.* Subplots show a TEM picture of the TiO_2 nanoparticles (**a**), quantification of total ad- and/or absorbed Ti at the nominal exposure concentrations (circles) (**b**), and quantification of phosphorus (P, squares), potassium (K, triangles) and silicon (Si, diamonds) (**c**). Mean and SEM concentrations of all quantified elements (n=6) are presented in Table S2.

Table 3.2: Mean hydrodynamic size and zeta potential of $nTiO_2$ aggregates over one day of incubation in egg water. Mean and standard error of the mean are presented (*n*=3).

	Exposure (mg $TiO_2 \cdot L^{-1}$)	*Incubation time (h)*		
		0	*1.5*	*24*
Hydrodynamic size (µm)	2	1.63 ± 0.40	1.31 ± 0.38	1.22 ± 0.38
	5	0.94 ± 0.12	1.00 ± 0.13	2.50 ± 0.89
	10	1.34 ± 0.19	1.55 ± 0.09	4.10 ± 1.08
Zeta potential (mV)	2	-18.9 ± 0.4	-18.4 ± 0.3	-19.8 ± 0.5
	5	-15.4 ± 1.6	-12.8 ± 0.5	-14.2 ± 2.3
	10	-6.5 ± 4.2	-9.9 ± 2.0	-13.5 ± 0.7

exposure concentrations, averaging 155 ± 34 ng at 5 mg $TiO_2 \cdot L^{-1}$ and 154 ± 21 ng at 10 mg $TiO_2 \cdot L^{-1}$ ($p=9.0 \cdot 10^{-6}$). The latter two concentrations did not differ significantly ($p>0.05$), suggesting that sorption of $nTiO_2$ had saturated at this concentration of sorbed Ti, averaging 153 ± 19 ng Ti (257 ± 32 ng TiO_2) per egg. Based on the size of the $nTiO_2$ aggregates determined by DLS (Table 3.2), the effective density of aggregates (0.328 $g \cdot cm^{-3}$) determined from TEM pictures (Fig. S2), and the radius of zebrafish eggs determined from CLSM images (0.6 mm), aggregates of this amount of $nTiO_2$ could cover 25.2 % of the egg surface in a hexagonal close-packing. In non-aggregated form, the corresponding number of primary particles could cover 44.8 % of the zebrafish egg surface.

Fifteen other elements were detected on zebrafish eggs, including phosphorus, chloride, potassium, sulfur, sodium, magnesium, manganese, calcium, silicon, iron, cobalt, chromium, zinc, aluminum and nickel (Table S2). Of all these elements, only the concentration of potassium correlated positively with the concentration of titanium ($r_s=0.45$, $n=24$, $p=0.03$). There was a slight but insignificant correlation between concentrations of titanium and phosphorus ($r_s=0.33$, $n=24$, $p=0.12$). The concentrations of silicon per egg correlated negatively with concentrations of titanium ($r_s=-0.46$, $n=24$, $p=0.02$) (Fig. 3.1c).

3.3.3 Internalization of nanoparticles by zebrafish eggs

In order to investigate if nanoparticles can be internalized by zebrafish eggs, we localized nAu on zebrafish eggs following 24 h of exposure by way of two-photon multifocal microscopy (Fig. 3.2). We firstly used CETAB-stabilized nanorods to study how nAu appears in two-photon images. Due to their high stability, these particles can be identified based on their TPL optimum at an excitation wavelength around 850 nm, resulting from plasmon resonance. nAu appeared as bright spots in two-photon images (Fig. 3.2a–c). Background fluorescence, as detected in images of non-exposed eggs, was visible as a blur comprising dim spots that lacked the characteristic emission optimum

(Fig. 3.2d–f). We subsequently used this information to localize PVP-coated nanorods with much lower toxicity, at increasing exposure concentrations. It was not possible to localize these rods based on their emission optima directly, because aggregation of these rods, resulting from their lower stability, can shift the wavelength of emission optima. In z-projections of zebrafish eggs exposed to increasing concentrations of nAu, increasing amounts of nAu could be detected on the surface of zebrafish eggs (Fig. 3.2g–l). Inside of the zebrafish eggs, a background blur was visible at the location of the head of the developing embryo. However, no bright spots corresponding to excited nAu could be detected inside of zebrafish eggs (Fig. 3.2i, Fig. S5).

3.3.4 Survival of microbiota on zebrafish eggs

Using fluorescence microscopy, ovoid and rod-shaped microbes could be identified on the surface of zebrafish eggs (Fig. 3.3a). Without exposure to $nTiO_2$, the microbes were spread homogeneously over the chorion, covering 0.43 ± 0.06 % of the total chorion surface. A 2-fold higher surface area of the chorion was covered by live microbes (0.29 ± 0.06 %) than by dead microbes (0.14 ± 0.01 %). However, this difference was not significant ($F_{1,79} = 1.48$, $p > 0.05$), possibly due to the required log-transformation of the data on coverage. Exposure to $nTiO_2$ resulted in a higher total cover of live and dead microbes on zebrafish eggs ($F_{1,127} = 7.77$, $p=0.006$) (Fig. 3.3b; Table S3). It moreover affected to ratio between the cover of dead and live microbes on the chorion. At 2 mg $TiO_2 \cdot L^{-1}$, dead microbes covered a larger surface area of zebrafish eggs than live microbes ($F_{1,41} = 8.58$, $p = 0.006$). In contrast, at 5 and 10 mg $TiO_2 \cdot L^{-1}$, equal surface areas were covered by dead and live microbes ($F_{1,41} = 1.52$, $p > 0.05$ and $F_{1,79} = 0.30$, $p > 0.05$, respectively).

The bacteria that could be isolated from zebrafish eggs belonged to five different genera (Fig. 3.3c, Table S4). Most (33) of the isolated 16S rRNA sequences had high sequence similarity (98-100 % identity) to sequences of identified bacterial species included in the NCBI database. The seven sequences with lower similarity (93–98 % identity) corresponded to the same bacterial species as the sequences with high similarity. Eggs of both $nTiO_2$-exposed and non-exposed conditions comprised bacteria of the genera *Aeromonas*, *Pseudomonas* and *Delftia*. The aeromonads had highest 16S rRNA sequence similarity to the species *A. hydrophila, A. sobria. A. salmonicida, A. veronii,* or *A. diversa*; the pseudomonads were most similar to *P. mosselii, P. putida, P. fluorescens, P. entomophila, P. hunanensis,* or *P.* cf. *monteilii*; and the *Delftia* bacteria had highest sequence similarity to either *D. lacustris* or *D. tsuruhatensis*. In addition to these genera, the bacteria *Chryseobacterium massiliae* and *Stenotrophomonas maltophilia* could be identified among bacterial isolates from exposed eggs.

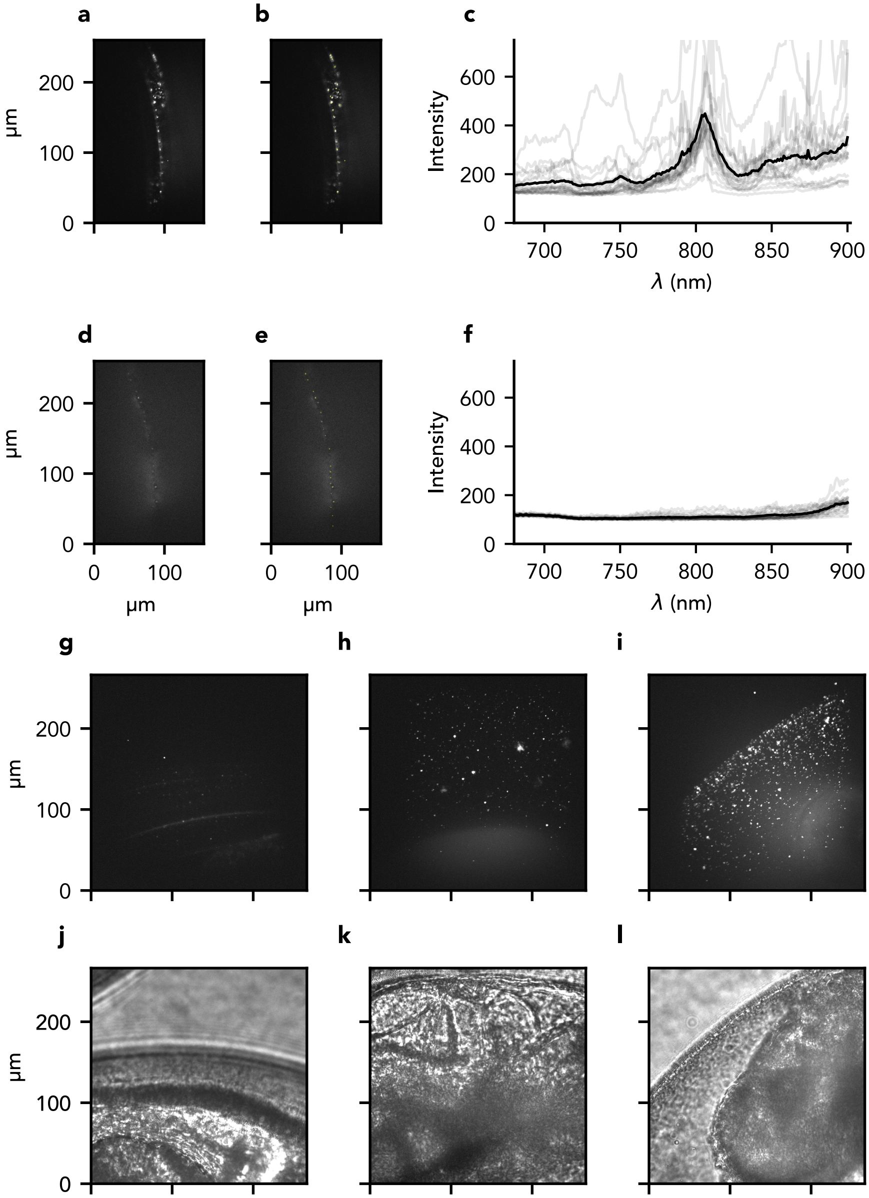

Figure 3.2: *Two-photon microscopy detection of gold nanorods on zebrafish eggs at 1 day post-fertilization.* Subplots show representative images of a zebrafish embryo following 24 h-exposure to 0.03 mg Au·L^{-1} CETAB-coated gold nanorods (**a**), with 20 regions of interest (ROIs) (**b**) used to obtain excitation spectra (**c**); a zebrafish embryo that had not been exposed to nanorods (**d**), with 20 ROIs (**e**) that were used to obtain excitation spectra (**f**); and z-projections of embryos that had been exposed for 24 h to no nanorods (**g**), 0.03 mg Au·L-1 PVP-coated gold nanorods (**h**), and 0.1 mg Au·L^{-1} PVP-coated gold nanorods (**i**). Transmitted light images **j**), **k**), and **l**) correspond to emitted light images **g**), **h**) and **i**), respectively. The black line in graph **c**) and **f**) depict the mean intensity of the intensity of all 20 ROIs, indicated with gray lines.

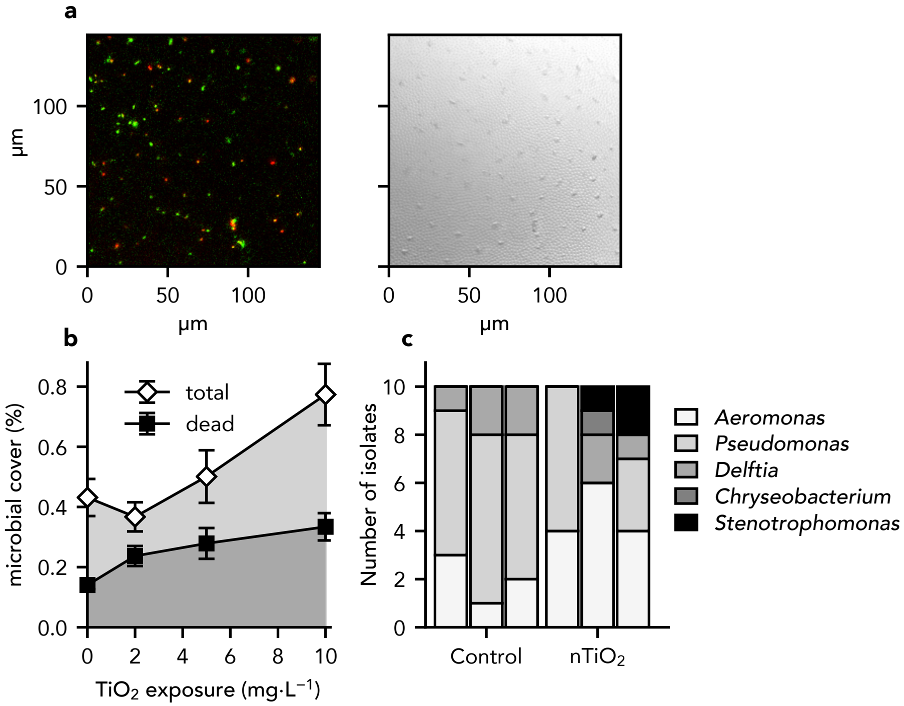

Figure 3.3: *Impacts of nTiO₂ on microbial communities establishing on zebrafish eggs.* Subplots show a CLSM picture of dead (red) and live (green) microbes (**a**, left picture) on the surface of a zebrafish egg (**a**, right picture); the impact of 24 h-exposure to nTiO₂ on total microbial cover (white diamonds) and dead microbial cover (black squares) on the surface of zebrafish eggs (*n*=24–45; mean ± SEM are presented) (**b**); and the identity of bacteria isolated from zebrafish eggs exposed for 24 h to no nanoparticles ('Control'; left bars) and 5 mg $nTiO_2 \cdot L^{-1}$ ('$nTiO_2$'; right bars). Each bar represents 10 bacterial isolates from 1 biological replicate. The corresponding BLAST results are included in Supplementary Table S4.

3.3.5 Cascading effects on microbiota of zebrafish larvae

All of the applied concentrations of $nTiO_2$ were sublethal to zebrafish larvae during 24 h of exposure (Fig. S6). Given the saturation of $nTiO_2$ on zebrafish eggs at an exposure concentration of 5 mg $TiO_2 \cdot L^{-1}$, we selected this embryonic exposure scenario to study potential cascading effects on larval microbiota abundance and composition. As a positive control, the highest sublethal concentration of nAg (0.25 mg $Ag \cdot L^{-1}$) was selected, which has previously been confirmed to exert high antimicrobial activity. In accordance with confocal microscopy results, exposure to $nTiO_2$ resulted in a significantly higher number of colony-forming units (CFUs) per egg than incubation in egg water without nanoparticles ($F_{1,13}=22.95$, $p=0.00035$) (Fig. 3.4, Table S3). From

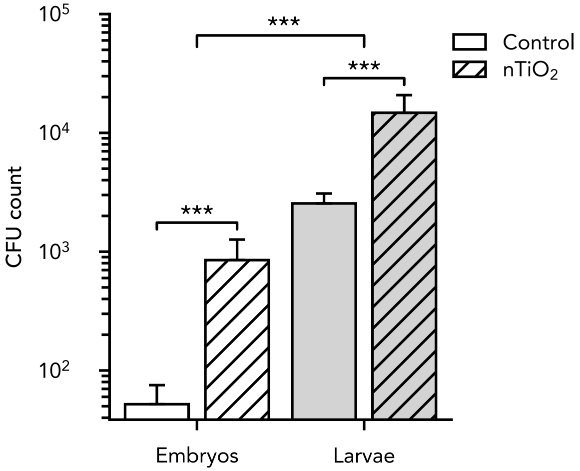

Figure 3.4: *Total count of colony-forming units* (CFUs) associated per zebrafish embryo (1 dpf; white bars) or per zebrafish larva (5 dpf; gray bars) following embryonic exposure (0-1 dpf) to egg water without nanoparticles ('Control'; non-hatched, white fill), and egg water comprising $nTiO_2$ (5 mg $TiO_2 \cdot L^{-1}$; hatched fill). Bars represent means with standard error of the mean (*n*=3). Asterisks indicate significant differences ($p<0.001$).

surrounding water without $nTiO_2$, a median number of $8.2 \cdot 10^2$ $CFUs \cdot mL^{-1}$ (IQR = $4.2 \cdot 10^2$–$1.8 \cdot 10^3$ $CFUs \cdot mL^{-1}$, n=23) could be isolated at 6 hpf, which corresponded to $1.6 \cdot 10^2$ $CFUs \cdot egg^{-1}$ (IQR = 83–$3.7 \cdot 10^2$ $CFUs \cdot egg^{-1}$, n=23). Larvae comprised higher numbers of CFUs than eggs ($F_{1,13}$=50.90, p=$3.5 \cdot 10^{-6}$). This difference in microbial abundance between the exposed and non-exposed group persisted until 5 dpf (Fig. 3.4; Table S3).

We used EcoPlates to assess the functional composition of heterotrophic zebrafish microbiota based on carbon substrate utilization. The activity of zebrafish enzymes did not interfere with this analysis, since carbon substrate utilization by germ-free larvae resulted in a negligible average well-color development (AWCD) of 0.007 ± 0.0008 in comparison to carbon substrate utilization of microbially colonized larvae (AWCD = 0.45 ± 0.01). In contrast to microbiota abundance, the functional composition of the zebrafish egg microbiota did not differ between exposed and non-exposed groups, as determined based on carbon substrate utilization ($F_{1,28}$=0.68, p>0.05; Fig. 3.5a, Fig. S8a). Larvae had a functionally distinct microbiota composition ($F_{1,28}$=11.21, p=0.001), which diverged slightly following exposure to $nTiO_2$, as indicated by a significant interaction between life stage and exposure ($F_{1,28}$= 5.63, p=0.001; Fig. 3.5a, Fig. S8b). However, compared to the effects of embryonic exposure to sublethal concentrations of nAg, impacts of sublethal concentrations of $nTiO_2$ on the functional microbiota composition of zebrafish larvae were minor (Fig. S8-S9). Accordingly, exposure to $nTiO_2$ did not result in differences in AWCD (0.45 ± 0.01; $F_{1,31}$= 0.27, *p*>0.05; Fig. 3.5b), the diversity in utilized carbon substrates ($F_{1,31}$= 0.57, *p*>0.05; 2.75 ± 0.017 in larvae and 2.63 ± 0.041 in eggs, $F_{1,31}$=15.0; *p*=0.0005; Fig.3.5c), and the richness in utilized carbon substrates (14.5 ± 0.34; $F_{1,31}$=1.34, *p*>0.05; Fig. 3.5d). For comparison, although nAg exposed and non-exposed larvae had similar microbiota abundance (Fig. S7), exposure to nAg resulted in significantly lower AWCD of larval microbiota (0.33 ± 0.02; $F_{2,22}$=18.13, *p*<0.0001; Fig. S8b). No difference in the diversity in utilized carbon substrates (2.77 ± 0.02; $F_{2,22}$=1.51, *p*=0.24; Fig. S8c) and richness of utilized carbon substrates (14.85 ± 0.40; $F_{2,22}$=0.055, *p*>0.05; Fig. S8d) of larval microbiota could be detected following exposure to nAg. The evenness of the egg and larval microbiota carbon substrate utilization could only be compared with care, as residuals did not follow a normal distribution, even following log or rank transformation. However, the carbon substrate utilization profile of embryos appeared to be slightly more even (1.00 ± 0.004) than that of larvae (1.02 ± 0.006; $F_{1,31}$=8.78, *p*=0.006). The evenness of larval microbiota carbon substrate utilization was not affected by exposure to $nTiO_2$ or nAg (1.03 ± 0.007; $F_{2,22}$=2.65, *p*>0.05; Fig. S8e).

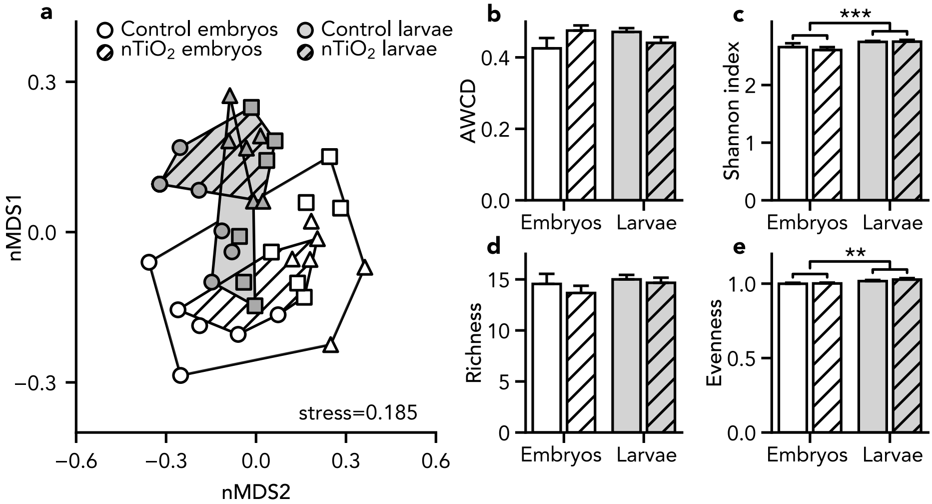

Figure 3.5: *Carbon substrate utilization characteristics of microbiota isolated from zebrafish embryos* (1 dpf) *and zebrafish larvae* (5 dpf) following embryonic exposure (0-1 dpf) to egg water without nanoparticles (non-hatched), and egg water comprising $nTiO_2$ (5 mg $TiO_2 \cdot L^{-1}$; hatched fill). Subplots represent carbon substrate utilization profiles (**a**), total well color development (TWCD) (**b**), Shannon index (**c**), richness (**d**), and evenness (**e**). Each biological replicate, comprising three measurement replicates, is depicted with a unique marker shape. Bars represent means with standard error of the mean (n=3). Asterisks indicate significant differences (**, *p*<0.01; ***, *p*<0.001).

3.4 Discussion

Teleost fish embryos, developing *ex vivo* in the water column, are protected against particulate pollutants by two acellular envelopes: the inner vitelline and the outer chorion membrane. Despite the efficacy of this physical barrier against particles in the environment, as confirmed in several studies (Böhme 2015; Van Pomeren et al. 2017a; Batel et al. 2018; Brun et al. 2018; Lee et al. 2019; Duan et al. 2020), the adsorption and enrichment of particles on the chorion surface has been related to several adverse effects. These include the obstruction of gas exchange across the chorion surface (Duan et al. 2020), and the leaching of toxic chemicals and ions out of chorion-attached particles into the eggs (Böhme 2015; Batel et al. 2018). Given the antimicrobial nature of many metal nanoparticles, and the importance of early microbial colonization to larval development (Rawls et al. 2004; Hill et al. 2016; Phelps et al. 2017), we hypothesized that the disruption of the chorion-attached microbial community constitutes a hitherto unexplored adverse effect of concern. In this study, we took a three-step approach to investigate this, focusing on the impacts of titanium dioxide nanoparticles on zebrafish embryos. Firstly, we inferred if the particles accumulated on the chorion surface; secondly, we studied how this affected the microbial community that establishes on the chorion surface; and thirdly, we examined if this resulted in any cascading effects on the larval microbial community.

3.4.1 Internalization of nanoparticles by zebrafish eggs

As a first step, we assessed if nanoparticles can cross the external membranes of zebrafish eggs, employing the advantages of two-photon microscopy for the localization of nAu. This approach builds on previous knowledge obtained using fluorescently labeled particles, or using destructive analyses such as Laser Ablation Inductively Coupled Plasma Mass Spectrometry (LA-ICP-MS), enabling live imaging without the risk of fluorescent dye dissociation, with less autofluorescence background than with the use of fluorophores, and providing a high z-confinement with large penetration depth (Van Den Broek 2013). Using this approach, we did not detect any particles inside of zebrafish eggs, yet observed a high and concentration-dependent accumulation of nanoparticles on the chorion surface. Considering the high sensitivity of two-photon microscopy detection of nAu, this suggests that the particles did not cross the chorion surface. Moreover, in view of the lower stability of $nTiO_2$ than nAu, resulting in larger aggregate sizes, it is even less likely that $nTiO_2$ aggregates can cross the chorion pores. These findings agree with previous results, showing an accumulation of polystyrene nanoparticles (Van Pomeren et al. 2017a; Duan et al. 2020), silicon nanoparticles (Fent et al. 2010), copper nanoparticles (Brun et al. 2018), titanium dioxide, silver, gold, and aluminum oxide nanoparticles (Osborne et al. 2013; Böhme et al. 2015) onto or inside of zebrafish chorions, with limited or no detectable uptake of particles by the embryos.

Using PIXE to quantify elemental concentrations of Ti, we observed a concentration-dependent accumulation of $nTiO_2$ onto zebrafish eggs, reaching a maximum of 154.3 ± 19.2 ng Ti (257.4 ± 32.0 ng TiO_2) per egg at a nominal exposure concentration of 5 mg $TiO_2 \cdot L^{-1}$. Previous studies have shown that small (1-5 μm) microplastic particles (Batel et al. 2018) and metal nanoparticles (Böhme 2015; Shih et al. 2016) can cover the zebrafish chorion completely. Although our estimates of the chorion coverage are lower, we nevertheless estimated that a relatively large surface of the chorion could be covered by TiO_2 aggregates (25.2 %) or primary particles (44.8 %), as compared to the surface of the chorion that is occupied by microbes (<1%). Studies applying more optimal sorption conditions, obtained even higher particle coverages. In an experimental setup where eggs were exposed to nanoparticles in a rotating glass vial, Shih et al. (2016) reached a maximum of 6 tightly bound layers of $nTiO_2$ in a hexagonal close-packing of primary particles. Comparably, Lin et al. (2015) calculated that 2–17 layers of primary TiO_2 particles attached to cells of algae *Raphidocelis subcapitata* in a hexagonal close-packing.

The accumulation of TiO_2 coincided with changes in the elemental concentrations of silicon and potassium of zebrafish eggs. Concentrations of Ti correlated negatively with silicon, which could result from competition in binding sites of Ti and silicon on the chorion, or from lower internalization rates of silicon by the TiO_2-exposed embryos. In view of indications for the contribution of silicon to immune and inflammatory responses, osteogenesis, and the formation of connective tissue (Nielsen 2014), the latter scenario merits further investigation.

A positive correlation was found between concentrations of Ti and potassium of zebrafish eggs. A similar, yet insignificant trend was observed for the concentration of phosphorus. Of all detected elements by PIXE (Table S2), potassium constitutes the most abundant element in bacteria, followed by phosphorus (Novoselov et al. 2013). This suggests that the higher concentrations of both potassium and phosphorus were detected on zebrafish chorions as a result of the accumulation of bacteria on zebrafish chorions.

3.4.2 Survival of microbiota on zebrafish eggs

To address our second research question, we characterized the effects of $nTiO_2$ on microbial consortia that establish on the chorion of zebrafish eggs. In accordance with the reported antimicrobial activity of $nTiO_2$, we detected a higher cover of dead microbes on the chorion surface of zebrafish eggs following exposure to $nTiO_2$.

However, imaging analyses also showed that exposure concentrations above 2 mg $TiO_2 \cdot L^{-1}$ resulted in an overall increase in total microbial abundance. For this reason, the antimicrobial effects of $nTiO_2$ could not have been identified using culture-dependent microbial techniques only. For future research, this shows the importance to support culture-dependent analysis of microbiota composition with culture-independent techniques to assess microbiota composition, specifically using microbial profiling techniques that are based on RNA, or include initial removal of relic DNA, to allow to distinguish dead from live microbiota (Knight et al. 2018).

Similar to our results, Zhai et al. (2019) detected a concentration-dependent increase in soil microbiota abundance following 24 h-exposure to $nTiO_2$, with higher microbial abundance at 500 and 2000 mg $TiO_2 \cdot kg^{-1}$ soil than at 0 and 1 mg $TiO_2 \cdot kg^{-1}$ soil. Nevertheless, these effects were of transient nature, and the adverse effects of $nTiO_2$ on microbial abundance gradually appeared from 15 to 60 days of exposure. In the present study, such adverse effects of prolonged exposure to $nTiO_2$ might explain why the acute growth-promoting effects of $nTiO_2$ did not result in higher AWCD over the two days longer Ecoplate incubations.

Following 24 h of exposure to 5 mg $TiO_2 \cdot L^{-1}$, over 16 times more CFUs were isolated from TiO_2-exposed embryos than from control embryos. One explanation to this difference could be potential growth-promoting effects of $nTiO_2$ on certain bacterial isolates; only four generation cycles are required to obtain a 16-times difference in microbial abundance. An alternative and non-exclusive explanation follows from our DLS results. Above exposure concentrations of 2 mg $TiO_2 \cdot L^{-1}$, we measured a more neutral zeta potential, and observed a corresponding increase in the hydrodynamic size of aggregates over time. This suggests that particle stability was lower at exposure concentrations above 2 mg $TiO_2 \cdot L^{-1}$. Accordingly, imaging analyses indicated that only at exposure concentrations above 2 mg $TiO_2 \cdot L^{-1}$, exposure to $nTiO_2$ resulted in higher microbial abundance on zebrafish eggs. Combined, these results may imply that the increased microbial abundance at exposure concentrations above 2 mg $TiO_2 \cdot L^{-1}$ resulted from the formation of heteroaggregates of microbes and TiO_2 in the water column, which subsequently settled onto zebrafish eggs. In agreement with this reasoning, the total number of CFUs in the water column without exposure to TiO_2 ($1.6 \cdot 10^2$ $CFUs \cdot egg^{-1}$; IQR = 83–$3.7 \cdot 10^2$ $CFUs \cdot egg^{-1}$, n=23), can explain a large part of the difference in CFU counts between non-exposed eggs (52 ± 23 $CFUs \cdot egg^{-1}$) and $nTiO_2$-exposed eggs ($8.5 \cdot 10^2 \pm 4.2 \cdot 10^2$ $CFUs \cdot egg^{-1}$). Heteroaggregation dynamics of $nTiO_2$ with microbes have already been described for the unicellular alga *R. subcapitata* (Lin et al. 2015). Moreover, the aggregation and subsequent sedimentation of microbes with suspended particles is a well-described phenomenon in the water column of pelagic water bodies, known as marine snow (Suzuki and Kato 1953) or lake snow (Grossart and Simon 1998).

3.4.3 Cascading effects on microbiota of zebrafish larvae

The third part of our study concerned the potential consequences of altered embryonic microbiota to zebrafish larvae health. Specifically, we inferred if $nTiO_2$-induced changes in chorion-attached microbiota resulted in different larval microbiota abundance and composition. Considering the potential functional redundancy of microbes, we used carbon substrate utilization as a functional measure of microbiota composition. We found that the higher microbial abundance on zebrafish eggs that had been exposed to $nTiO_2$, persisted until the 5 dpf-larval stage. This indicates that microbes which grow on zebrafish eggs as a result of $nTiO_2$ exposure, possibly due to the adsorption of aggregates consisting of microbes and $nTiO_2$ onto the chorion surface, can colonize the larvae upon hatching. In our experiment, this did not result in different functional composition of larval microbiota, as determined based on carbon-substrate utilization. However, there is a risk that hazardous microbes are transferred to eggs following heteroaggregate formation in aquatic ecosystems. In the Baltic Sea, for instance, potentially pathogenic *Vibrio* bacteria have been identified on microplastic particles (Kirstein et al. 2016). Of comparable concern, we identified *Aeromonas* species on zebrafish eggs which are known to be pathogenic to fish (Fernández-Bravo and Figueras 2020), which were one of the species *A. hydrophila* (infecting salmonids and eel), *A. salmonicida* (infecting salmonids), *A. sobria* (infecting tilapia and common carp) or *A. veronii* (infecting catfish, common carp, and eel). More broadly, aeromonads have been associated with infections in echinoderms, mollusks, copepods, crocodiles, frogs, rabbits, cats, dogs, horses and humans (Fernández-Bravo and Figueras 2020). The presence of these aeromonads on $nTiO_2$-exposed eggs suggests that these bacteria are able to cope with the particles' antimicrobial properties. Therefore, it is possible that pathogenic aeromonads are transferred throughout aquatic ecosystems, and to aquatic eggs, via attachment to suspended $nTiO_2$ particles and aggregates.

Although the nAg-exposed eggs of the positive control developed functionally different larval microbiota than zebrafish eggs that had not been exposed to nanoparticles, larval microbiota of $nTiO_2$-exposed eggs did not differ from non-exposed eggs in carbon substrate utilization. This lower impact of $nTiO_2$ on microbiota composition, as compared to nAg, at concentrations that are sublethal to the host, has been reported for soil microbes (Ahmed et al. 2020), intestinal microbiota of mice (Chen et al. 2017), and human gut simulator microbiota (Agans et al. 2019). Nevertheless, even though we exclusively isolated the bacteria *C. massiliae* and *S.*

maltophilia from $nTiO_2$-exposed eggs, which could indicate that the composition of exposed and non-exposed egg microbiota differed taxonomically, also microbiota of eggs did not differ in carbon substrate utilization profiles. This may imply that $nTiO_2$-exposure can induce shifts in microbiota composition that do not result in different microbiota functioning, as a result of functional redundancy. Interestingly, Zhai et al. (2019) obtained similar results for the impacts of $nTiO_2$ on soil microbiota. This remarkable similarity in the impacts of $nTiO_2$ on microbiota from different environments warrants further research, investigating the generalizability of these results.

On a similar note, comparing the particle-specific protection of the external structures surrounding the embryos of different taxa merits further investigation. At a large phylogenetic distance to teleost fish, for instance, it can be questioned if egg coatings facilitate early microbial colonization, given the bactericidal or bacteriostatic activity of the jelly layer of amphibian eggs (Mazzini et al. 1984). Even at low phylogenetic distances, a remarkable diversity of egg surfaces exists. Demersal fish, for example, generally produce eggs with much thicker and harder chorion structures than pelagic fish (McMillan 2007). Moreover, chorions can have diverse kinds of protrusions, such as threads, fibrils, or spikes, increasing their surface area. Additionally, differences between the environments where these eggs develop – including turbidity, water column depth, currents, salinity, and the presence of other pollutants or stressors – will affect the interactions between suspended particles and microbiota colonizing aquatic eggs externally. In view of this diversity in the external surface and environment of aquatic eggs, the adverse effects of nanoparticle adsorption on the eggs of oviparous animals, as examined in this study, may contribute to variation in nanoparticle sensitivity across different taxa. Further characterization thereof may help to refine the assessment of environmental risks of nanoparticle exposure on early life stages of oviparous animals.

3.5 Conclusions

Early host-microbiota interactions are of key importance to the development of zebrafish larvae. In this study, we tested the hypothesis that the adsorption of antimicrobial titanium dioxide nanoparticles on zebrafish eggs can perturb microbial communities that establish on the egg surface, indirectly affecting the subsequent colonization of hatched larvae. Our results confirmed that both nanoparticles and microbes accumulated on the surface of zebrafish eggs, whereas no particles could be detected inside of the eggs. At increasing exposure concentrations, this resulted in higher dead and total microbial abundance, and altered concentrations of potassium and silicon. These impacts of titanium dioxide nanoparticles on egg microbiota had cascading effects on later life stages, as indicated by a persisting increased microbial abundance of larvae. Combined with measurements on particle stability, this overall stimulatory effect of nTiO$_2$ on egg- and larval microbial abundance can potentially be explained by the formation of heteroaggregates of microbes and nanoparticles that settle on the egg surface. Given the tolerance of pathogenic aeromonads against antimicrobial properties of titanium dioxide particles, these dynamics potentially come at the expense of increased dispersal of pathogenic bacteria through aquatic ecosystems, as well as across different life stages of oviparous animals.

Author contributions

Bregje W. Brinkmann: Conceptualization, Investigation, Supervision, Formal analysis, Writing – Original Draft, Review & Editing. ***Wouter F. Beijk***: Investigation, Methodology, Writing – Review & Editing. ***Redmar C. Vlieg***: Investigation, Methodology, Writing – Review & Editing. ***S. John T. van Noort***: Supervision, Funding acquisition, Writing – Review & Editing. ***Jorge Mejia***: Investigation, Methodology, Writing – Review & Editing. ***Julien L. Colaux***: Investigation, Methodology, Writing – Review & Editing. ***Stéphane Lucas:*** Supervision, Funding acquisition. ***Gerda Lamers***: Methodology, Writing – Review & Editing. ***Willie J. G. M. Peijnenburg***: Supervision, Writing – Review & Editing. ***Martina G. Vijver***: Supervision, Funding acquisition, Writing – Review & Editing.

Data availability statement

Data is available via Mendeley Data: DOI:10.17632/2d4hcr5cb5.1

Supporting material is made available by *Aquatic Toxicology* [online]:
DOI: 10.1016/j.aquatox.2021.105744

Acknowledgements

We thank Ilaria Zanoni for performing the nTiO$_2$ sedimentation measurements, Rian van den Nieuwendijk for providing technical support and equipment for the lyophilization of zebrafish eggs; Emilie Didaskalou for help with the concerning sample preparation; and RAS AG for providing the applied silver nanoparticles. John van Noort and Redmar Vlieg were supported by the Netherlands Organization for Scientific Research [VICI 680.47.616]. This work was supported by the project PATROLS of European Union’s Horizon 2020 research and innovation programme [grant number 760813].